Superconductivity of LaH$_{10}$ and LaH$_{16}$ polyhydrides

Ivan A. Kruglov [1,2,*] Dmitrii V. Semenok,[3,†] Hao Song,[4] Radosław Szczęśniak,[5,6] Izabela A. Wrona,[5] Ryosuke Akashi,[7] M. Mahdi Davari Esfahani,[8] Defang Duan,[4] Tian Cui,[4] Alexander G. Kvashnin,[3,1] and Artem R. Oganov[3,1,2,9,‡]

[1]*Moscow Institute of Physics and Technology, 9 Institutsky Lane, Dolgoprudny 141700, Russia*
[2]*Dukhov Research Institute of Automatics (VNIIA), Moscow 127055, Russia*
[3]*Skolkovo Institute of Science and Technology, Skolkovo Innovation Center, 3 Nobel Street, Moscow 121205, Russia*
[4]*Key State Laboratory of Superhard Materials, College of Physics, Jilin University, Changchun, China*
[5]*Institute of Physics, Jan Dlugosz University in Częstochowa, Ave. Armii Krajowej 13/15, 42–200 Częstochowa, Poland*
[6]*Institute of Physics, Częstochowa University of Technology, Ave. Armii Krajowej 19, 42–200 Częstochowa, Poland*
[7]*University of Tokyo, 7-3-1 Hongo, Bunkyo, Tokyo 113–8654, Japan*
[8]*Department of Geosciences and Center for Materials by Design, Institute for Advanced Computational Science, State University of New York, Stony Brook, New York 11794-2100, USA*
[9]*International Center for Materials Discovery, Northwestern Polytechnical University, Xi'an 710072, China*

Recent experiments have established previously predicted LaH$_{10}$ as the highest-temperature superconductor, with T_C up to 250–260 K [Drozdov *et al.*, Nature (London) **569**, 528 (2019); Somayazulu *et al.*, Phys. Rev. Lett. **122**, 027001 (2019)]. In this work we explore the high-pressure phase stability and superconductivity of lanthanum hydrides LaH$_m$. We predict the stability of the hitherto unreported polyhydride $P6/mmm$-LaH$_{16}$ at pressures above 150 GPa; at 200 GPa, its predicted superconducting T_C is 156 K, the critical field $\mu_0 H_C(0)$ is approximately 35 T, and the superconducting gap is up to 35 meV. We revisit the superconductivity of LaH$_{10}$ and find its T_C to be up to 259 K at 170 GPa from solving the Eliashberg equation and 271 K from solving the gap equation within the superconducting density functional theory, which also allows us to compute the Coulomb pseudopotential μ^* for LaH$_{10}$ and LaH$_{16}$.

I. INTRODUCTION

Recently, superhydrides (i.e., hydrides with excess of hydrogen relative to compositions expected from atomic valences) of various elements attracted great attention: they were first predicted and then experimentally proven to exhibit a record high-temperature superconductivity under a high pressure. According to Bardeen-Cooper-Schrieffer theory, metallic hydrogen is expected to be a high-T_C superconductor [1–4], yet the pressure needed for its formation is too high (∼500 GPa) [5]. Ashcroft proposed to stabilize states similar to metallic hydrogen at lower pressures by creating hydrogen-rich hydrides, where due to chemical interactions hydrogen atoms experience an additional "chemical" pressure [6]. Following this, many theoretical predictions of remarkable high-temperature superconductors were made, e.g., in the Ca-H [7], Y-H [8], H-S [9], Th-H [10], Ac-H [11], and La-H [8] systems. In all these systems, high-T_C superconductors have unusual chemical compositions, like H$_3$S, LaH$_{10}$, or CaH$_6$. The formation of such compounds, violating the rules of classical chemistry, commonly takes place under pressure [12].

Experimental proof was obtained for H$_3$S with measured $T_C = 203$ K at 155 GPa [13] (the predicted value was 191–

204 K at 200 GPa [9]). The confidence in such predictions has greatly increased because of their agreement with the observations, stimulating a wave of theoretical studies of superconductivity in hydrides [7,8,10,11,14–26]. Recent theoretical work on La-H and Y-H systems [8] under pressure showed that at 300 GPa LaH$_{10}$ and YH$_{10}$ may display room-temperature superconductivity (at 286–326 K). According to that theoretical study, at pressures below 200 GPa LaH$_{10}$ has the $R\bar{3}m$ symmetry, which changes to $Fm\bar{3}m$ at higher pressures. In the experiments by Geballe *et al.* [18], $R\bar{3}m$-LaH$_{10}$ was found at ⩽160– 170 GPa, while $Fm\bar{3}m$-LaH$_{10}$ was seen at higher pressures. The experimentally observed sharp drop in resistivity in the LaH$_{10}$ samples was the first evidence of superconductivity in this system [27,28]. Different studies showed a series of superconducting-like transitions with T_C of 70 and 112 K [27], 210–215 K [27], 244–250 K [27,28], and 260–280 K [27]. This discrepancy in the T_C values may be caused by the coexistence of lanthanum hydrides having different compositions and crystal structures in the studied samples. To obtain deeper understanding of the La-H system and rationalize experimental results, we predicted the stable compounds in the La-H system using the variable-composition evolutionary algorithm Universal Structure Predictor: Evolutionary Xtallography (USPEX) [29–31]. While most studies report only T_C and assume $\mu^* = 0.1$–0.15 for the calculations, here we obtain T_C using various approaches including the superconducting DFT, which requires no assumption of μ^*, and also compute other properties, such as the critical magnetic field [27].

*Corresponding author: ivan.kruglov@phystech.edu
†dmitrii.semenok@skoltech.ru
‡a.oganov@skoltech.ru

II. COMPUTATIONAL DETAILS

The evolutionary algorithm USPEX [29–31] is a powerful tool for predicting thermodynamically stable compounds of given elements. To predict thermodynamically stable phases in the La-H system, we performed variable-composition crystal structure searches at pressures from 50 to 200 GPa. The first generation of 100 structures was created using random symmetric [31] and topological structure generators [32] with the number of atoms in the primitive unit cell ranging from 8 to 16, while the subsequent generations contained 20% of random structures, and the remaining 80% of structures were created using the heredity, softmutation, and transmutation operators. Here, the evolutionary searches were combined with structure relaxations using density functional theory (DFT) [33,34] within the generalized gradient approximation [the Perdew-Burke-Ernzerhof (PBE) functional] [35], and the projector-augmented wave method [36,37] as implemented in the Vienna *ab initio* simulation package (VASP) [38–40]. The plane wave kinetic energy cutoff was set to 500 eV and the Brillouin zone was sampled by Γ-centered k-point meshes with the resolution of $2\pi \times 0.05\,\text{Å}^{-1}$. This methodology was used and proved to be very effective in our previous works (e.g., Refs. [10–12]).

The calculations of the critical temperature and electron-phonon coupling (EPC) parameters were carried out using the QUANTUM ESPRESSO (QE) package [41] within density functional perturbation theory [42], employing the plane-wave pseudopotential method and PBE exchange-correlation functional [35]. Convergence tests showed that 90 Ry is a suitable kinetic energy cutoff for the plane wave basis set. The electronic band structures and phonon densities of states were calculated using both VASP (the finite displacement method using PHONOPY [43,44]) and QE (the density functional perturbation theory [42]), showing good consistency of the results of these codes.

In our calculations of the EPC parameter λ, the first Brillouin zone was sampled using a $4 \times 4 \times 4$ q-point mesh and a denser $16 \times 16 \times 16$ k-point mesh (with the Gaussian smearing $\sigma = 0.02$ to improve convergence).

For LaH$_{10}$ and LaH$_{16}$, we also estimated T_C by solving the gap equation within the superconducting density functional theory (SCDFT) [45,46]:

$$\Delta_{nk}(T) = -Z_{nk}(T)\Delta_{nk}(T) - \frac{1}{2}\sum K_{nkn'k'}(T)$$
$$\times \frac{\tanh\beta E_{n'k'}}{E_{n'k'}}\Delta_{n'k'}(T). \tag{1}$$

Here, $E_{nk} = \sqrt{[\Delta_{nk}(T)]^2 + [\xi_{nk}]^2}$, with ξ_{nk} being the normal-state energy eigenvalue of $\hat{H}_e$ labeled by the band index n and wave vector k measured from the Fermi level. The "order parameter" $\Delta_{nk}(T)$ depends on n and k, not on the frequency ω; it is defined in a different way from that in the Eliashberg equation and is proportional to the thermal average $c_{nk\uparrow}c_{n-k\downarrow}$, with $c_{nk\sigma}$ being the annihilation operator of the spin state $nk\sigma$ [45]. The interaction effects treated in the Eliashberg equation are included with the kernels entering this gap equation; $Z_{nk} = Z_{nk}^{ph}$; $K_{nkn'k'} = K_{nkn'k'}^{ph} + K_{nkn'k'}^{el}$. Here we included the mass renormalization by the phonon exchange with $Z_{nk}^{ph} = Z^{ph}(\xi_{nk})$

(see Eq. (40) in Ref. [47] and an improved form of Eq. (24) in Ref. [46] to consider the nonconstant electronic density of states), the phonon-mediated electron-electron attraction with $K_{nkn'k'}^{PH} = K^{PH}(\xi_{nk}, \xi_{n'k'})$ (Eq. (23) in Ref. [46]), and the screened Coulomb repulsion $K_{nkn'k'}^{el}$ (Eq. (3) in Ref. [48]). Unlike the Eliashberg equation, the SCDFT gap equation does not contain the frequency ω. Nevertheless, the retardation effect [49] is approximately incorporated [46]. The absence of ω enables us to treat all electronic states in a wide energy range of ± 30 eV at an affordable computational cost, and therefore estimate T_C without the empirical Coulomb pseudopotential μ^*. We estimated T_C as the temperature where the nontrivial solution of this gap equation vanishes (see Supplemental Material [50]).

The Coulomb pseudopotential μ^*, included in the Eliashberg equation and its approximate solutions such as the Allen-Dynes (A-D) formula, quantifies the impact of the renormalized Coulomb repulsion. Its value can, in principle, be estimated from the matrix element of the screened Coulomb interaction and energy scales of the electrons and phonons [49,50], but practically it is determined by fitting the calculated observables to the experimental data or simply by accepting the typical values (e.g., ~0.10–0.15) from such previous fitting results [48]. On the other hand, while SCDFT gives us the framework free from empirical parameters such as μ^*, deriving from it some interesting observables is difficult compared with the Eliashberg theory. Especially, the spectral gap at absolute zero, being defined within the Green's function framework, is not directly accessible within SCDFT. To estimate several observable quantities, we took a hybrid approach reconciling these frameworks: determining the value of μ^* so that the Eliashberg (or A-D) equation reproduces T_C derived from the SCDFT gap equation [51] and then employing it in later calculations within Eliashberg theory. In this approach, we presume that the retardation effect [49] can be expressed by a single parameter, μ^*; possible drawbacks of this method are discussed later.

In this work we did not consider the effect of anharmonicity on the dynamic and superconducting properties of lanthanum hydrides. While this effect can be important, previous studies showed that the superconducting properties predicted within the "conventional" approach are in relatively good agreement with the experimental data.

III. RESULTS AND DISCUSSION

A. Stability of La-H phases

We performed variable-composition evolutionary searches for stable compounds and crystal structures at 50, 100, 150, and, 200 GPa. Thermodynamic convex hulls are shown in Fig. 1. By construction of the convex hull, stable phases are those that appear on the convex hull. Thus, at 50 GPa we found $Fm\bar{3}m$-LaH, $Pnma$-LaH$_3$, $Cmc2_1$-LaH$_7$, and Cc-LaH$_9$ to be stable [Fig. 1(a)]. At 100 GPa, LaH$_7$ and LaH$_9$ disappear from the convex hull, while four new hydrides become stable: Cm-LaH$_2$, $Cmcm$-LaH$_3$, $P\bar{1}$-LaH$_5$, and $P4/nmm$-LaH$_{11}$ [Fig. 1(b)]. At 150 GPa, the chemistry of lanthanum hydrides is much richer: $P6/mmm$-LaH$_2$, $Cmcm$-LaH$_3$, $I4/mmm$-LaH$_4$, $P\bar{1}$-LaH$_5$,
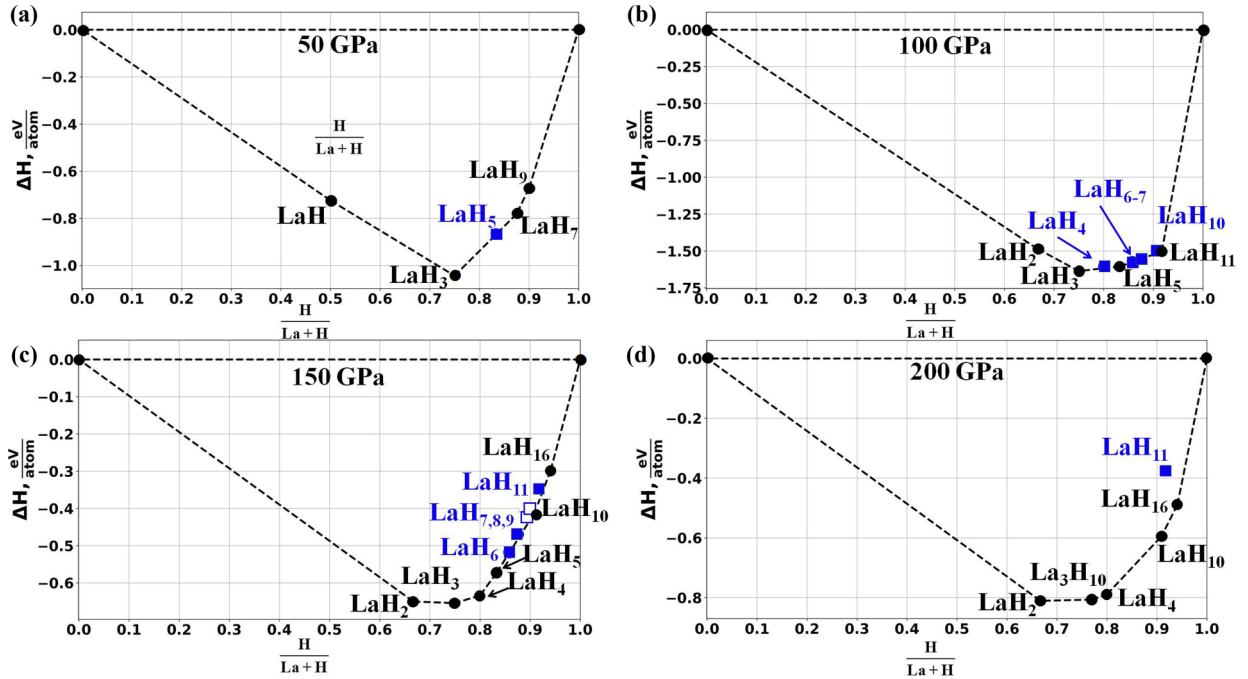
FIG. 1. Convex hull diagrams for the La-H system at (a) 50, (b) 100, (c) 150, and (d) 200 GPa. The metastable and stable phases are marked by blue squares and black circles, respectively.

$Fm\bar{3}m$-LaH$_{10}$, and $P6/mmm$-LaH$_{16}$ phases become stable [Fig. 1(c)]. At 200 GPa, only five stable lanthanum hydrides remain on the convex hull: $P6/mmm$-LaH$_2$, $Cmmm$-La$_3$H$_{10}$, $I4/mmm$-LaH$_4$, $Fm\bar{3}m$-LaH$_{10}$, and $P6/mmm$-LaH$_{16}$. Our results are similar to those from Ref. [52], the main difference being that we predict the new LaH, La$_3$H$_{10}$, and LaH$_{16}$ compounds and also find that LaH$_{10}$ is stable at pressures above 135 GPa, which is consistent with the experimental data [27,28]. Yet, we found $Fm\bar{3}m$-LaH$_{10}$ to be more stable than $R\bar{3}m$-LaH$_{10}$ at pressures above 150 GPa. The $R\bar{3}m \rightarrow Fm\bar{3}m$ phase transition occurs at 128 GPa (Supplemental Material Fig. S19 [50]). Taking into account the zero-point energy correction, the pressure of this phase transition shifts to 135 GPa, which is consistent with the experimental phase transition pressure of 160 GPa [18]. Below we discuss the superconducting properties of the previously known lanthanum hydrides and explore the crystal structure and SC properties of the newly found LaH$_{16}$. The crystal structure data are summarized in Supplemental Material Table S1 [50].

Stoichiometry 1:1 is common for various hydrides (e.g., U-H [12], Fe-H [21], and many others [53]). $Fm\bar{3}m$-LaH has a rocksalt-type structure, with La–H distance of 2.26 Å at 50 GPa. In the $Pnma$-LaH$_3$ structure, the La atoms have a tenfold coordination and H–H distances are too long to be considered bonding (2.28 Å at 50 GPa). In $Cmc2_1$-LaH$_7$, lanthanum atoms have a 13-fold coordination, while the shortest H–H distances (0.81 Å at 50 GPa) are clearly bonding and quite close to the H–H bond length in molecular hydrogen (0.74 Å).

Our results at 150 GPa are consistent with those in Ref. [8]: $P6/mmm$-LaH$_2$, $Cmcm$-LaH$_3$, $Immm$-LaH$_4$, and $P\bar{1}$-LaH$_5$ phases are thermodynamically stable. Previous studies explored only simple fixed stoichiometries, whereas the US-PEX method used here can automatically detect even non-

trivial stoichiometries, which helped us find a new phase, $Cmmm$-La$_3$H$_{10}$, at 200 GPa. This phase is structurally related to $Cmcm$-LaH$_3$, has an additional hydrogen atom in the tripled unit cell, and its lattice parameter c is three times larger.

Superconducting properties for the most promising LaH$_{10}$ and LaH$_{16}$ phases were calculated using the SCDFT method, then the μ^* value was determined by adjusting T_C obtained through the numerical solution of the Eliashberg equation to that from the SCDFT. For comparison, the μ^* values determined using the A-D formula are presented in Supplemental Material Table S2 [50]. We find a significant difference in the μ^* values obtained, depending on whether the Eliashberg or A-D equation were used, because the LaH$_x$ systems are classified as the strong-coupling case where these equations give substantially different values of T_C [27,48,54].

B. Superconductivity of LaH$_{10}$ phases

Superconductivity of LaH$_{10}$ has been confirmed in experiments [27,28]. Our analysis is based on the T_C calculation using the SCDFT, Eliashberg function $\alpha^2F(\omega)$, and the electronic density of states for $R\bar{3}m$- and $Fm\bar{3}m$-LaH$_{10}$ phases. The experimental observations found the maximum $T_C \sim 251$ K at 168 GPa [28] or $T_C \sim 260$ K at 180 GPa [27], which is close to the $R\bar{3}m$-$Fm\bar{3}m$ phase transition (but in the cubic phase). The value of the Coulomb pseudopotential μ^* for the LaH$_{10}$ phases determined using the SCDFT equals 0.2 at 200 GPa (see Supplemental Material [50]).

For $Fm\bar{3}m$-LaH$_{10}$, the calculations within the DFPT give a very high EPC coefficient $\lambda = 3.75$, which leads to $T_C = 271$ K at 200 GPa (see Table I and Supplemental Material for details [50]). At 200 and 250 GPa, the calculated volumes (30.4 and 28.5 Å^3, respectively) and the electronic density

TABLE I. Parameters of the superconducting state of $Fm\bar{3}m$-LaH$_{10}$ and $R\bar{3}m$-LaH$_{10}$ from the Eliashberg equation, with $\mu^* = 0.2$, SCDFT (see Supplemental Material [50]).

Parameter	$Fm\bar{3}m$-LaH$_{10}$				$R\bar{3}m$-LaH$_{10}$	
	170 GPa	200 GPa	210 GPa	250 GPa	150 GPa	165 GPa
N_f, states/f.u./Ry	11.2	10.6	10.3	10.0	12.2	11.0
λ	3.94	3.75	3.42	2.29	2.77	2.63
$\omega_{\log}$, K	801	906	851	1253	833	840
T_C, K	259	271	249	246	203	197
$\Delta(0)$, meV	62.0	63.7	59.6	48.0	48.5	43.7
$\mu_0 H_C(0)$, T[a]	89.0	95.0	81.0	66.7	72.7	71.0
$\Delta C/T_C$, mJ/mol K^2	31.5	44.7	34.5	33.4	42.8	25.7
γ, J/mol K^2	0.019	0.016	0.015	0.011	0.018	0.018
$R_\Delta = 2\Delta(0)/k_B T_C$	5.54	5.46	5.55	5.00	5.55	5.54

[a]The experimentally measured critical magnetic field is 95–136 T [27].

of states, $N(E_F) = N(0) = 10.6$ and 10.0 states/f.u./Ry, allowed us to estimate the Sommerfeld constant (Table I) as 0.016 and 0.011 J/mol K^2, which is very close to that of $Fm\bar{3}m$-ThH$_{10}$ (0.011 J/mol K^2 [10]) at 100 GPa [55]. These constants were used to calculate the critical magnetic field [$\mu_0 H_C(0)$] and the jump in specific heat $\Delta C/T_C$ (Table I). The computational details are presented in Supplemental Material [50].

The Eliashberg function for the cubic $Fm\bar{3}m$-LaH$_{10}$ at 200 GPa is shown in Fig. 2(e) (for other pressure values and phases, see Supplemental Material [50]). The numerical solution of the Eliashberg equation for the cubic LaH$_{10}$ at the experimental pressure of 170 GPa results in $T_C = 259$ K

(Table I), which is in close agreement with the theoretical results [8] and experiments [27,28].

The calculated critical temperature for $R\bar{3}m$-LaH$_{10}$ at 150 GPa is 203 K (Table I), much lower than that of the $Fm\bar{3}m$ modification, which can explain the experimental results of Drozdov *et al.* [27].

The isotope coefficient β was calculated using the A-D formula (see Supplemental Material [50]). With $\mu^* = 0.11$ used for the A-D equation, the calculated value was the same, $\beta = 0.48$, for both $Fm\bar{3}m$-LaH$_{10}$ and $R\bar{3}m$-LaH$_{10}$ at 200 GPa. Using the isotope coefficient β, the critical temperature of lanthanum decadeuteride can be determined as $T_D = 2^{-\beta} T_H$, resulting in 181 K for $Fm\bar{3}m$-LaD$_{10}$ and 154 K for $R\bar{3}m$-LaD$_{10}$.
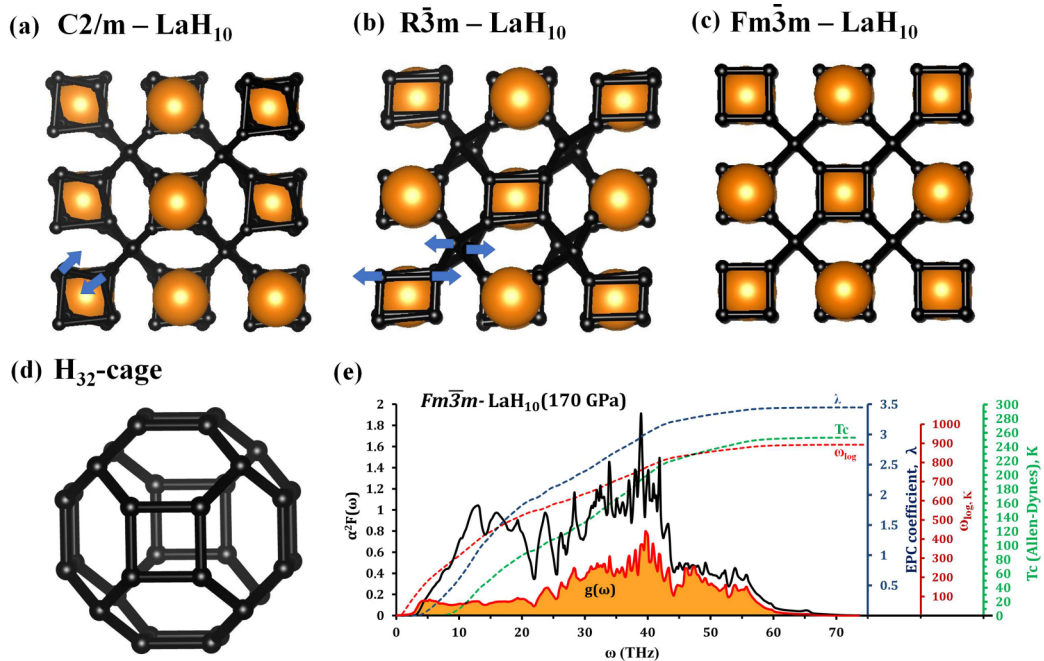

(a) C2/m − LaH$_{10}$ **(b) R$\bar{3}$m − LaH$_{10}$**   **(c) Fm$\bar{3}$m − LaH$_{10}$**

(d) H$_{32}$-cage   **(e)**

FIG. 2. Crystal structures of (a) $C2/m$-LaH$_{10}$, (b) $R\bar{3}m$-LaH$_{10}$, (c) $Fm\bar{3}m$-LaH$_{10}$, and (d) hydrogen H$_{32}$ cage common for these phases; (e) the Eliashberg $\alpha^2 F(\omega)$ function (black curve), phonon density of states (orange), cumulative $\omega_{\log}$ (red), EPC coefficient λ (blue), and critical transition temperature T_C (green) of $Fm\bar{3}m$-LaH$_{10}$ at 170 GPa. The crystal structures were generated using VESTA software [56]; the atoms of La and hydrogen are shown as large orange and small black balls, respectively; blue arrows show displacements of the hydrogen atoms away from their positions in a perfect cubic H$_8$ cluster.
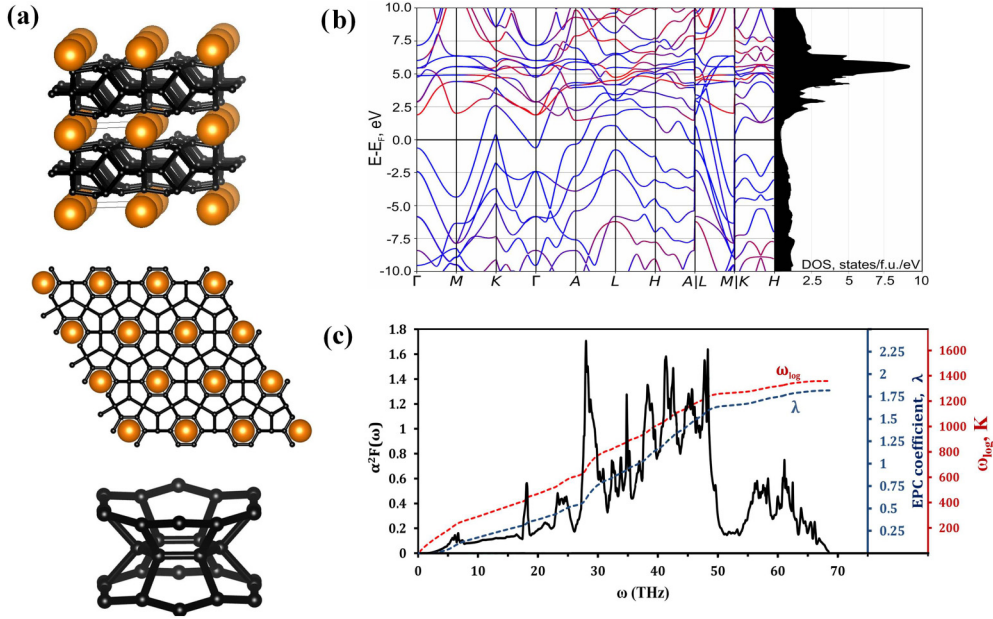
FIG. 3. (a) Crystal structure of $P6/mmm$-LaH$_{16}$ at 150 GPa; (b) band structure and DOS of LaH$_{16}$ (red lines are for La, blue lines are for H) at 250 GPa; (c) the Eliashberg function α^2F(ω) (black), cumulative $\omega_{\log}$ (red), and the EPC coefficient λ (blue) of $P6/mmm$-LaH$_{16}$ at 200 GPa.

The experimentally measured T_C for $Fm\bar{3}m$-LaD$_{10}$ is 168 K [27], close to our prediction.

C. Prediction of high-T_C LaH$_{16}$

Perhaps the most intriguing finding of our work is the prediction of thermodynamic stability of $P6/mmm$-LaH$_{16}$ at pressures above 150 GPa [Fig. 1(c)]. This phase has a crystal structure different from the previously predicted AcH$_{16}$ [11]. The lanthanum atoms form an hcp sublattice and are coordinated by 12 hydrogen atoms [Fig. 3(a)]. These H units consist of three parallel layers of hydrogen atoms. The distances between the hydrogen atoms in the first, second, and third layers at 150 GPa are 1.07, 1.02, and 1.07 Å, respectively. The distance between the closest hydrogen atoms from different layers is 1.25 Å, so these layers form infinite 2D networks. The crystal structures of all predicted phases are summarized in Supplemental Material Table S1 [50].

$P6/mmm$-LaH$_{16}$ shows very little dependence of the electronic density of states on the pressure at 200–300 GPa. The Eliashberg function of $P6/mmm$-LaH$_{16}$ computed at 200 GPa is shown in Fig. 3(c) (for other pressure values, see Supplemental Material [50]). The EPC coefficient of LaH$_{16}$ (Table II) is approximately two times lower than that of LaH$_{10}$. SCDFT calculations for LaH$_{16}$ at 200 GPa yield $T_C = 156$ K, which leads to the calculated $\mu^* = 0.41$, an anomalously large value compared to the commonly accepted 0.1–0.15 interval. This abnormal value of μ^* for LaH$_{16}$ is caused by the complex behavior of density of states (DOS)(E) in the energy range $E_F \pm 1$ eV (see Supplemental Material [50]). We used $\mu^* = 0.41$ in the numerical solution of the Eliashberg equation to calculate the superconducting properties of $P6/mmm$-LaH$_{16}$ (Table II). T_C of this phase shows a weak pressure dependence ($dT_C/dP = -0.3$ K/GPa).

Table III shows the critical temperatures for LaH$_{10}$ and LaH$_{16}$ calculated using SCDFT and the values of μ^* adjusted so that the Eliashberg equation and A-D formula give the same values of T_C.

D. Superconductivity of LaH$_m$ ($m = 4, …, 9, 11$)

It was shown before that different lanthanum hydrides can undergo a series of superconducting transitions with different T_C [27], so we checked other lanthanum hydrides to explore this possibility. In this work, we found a number of LaH$_m$ phases ($m = 4, …, 9, 11$) at different pressures, and calculating their T_C using SCDFT or the numerical solution of the Eliashberg equation would be computationally very expensive. Therefore, we calculated T_C of LaH$_m$ phases ($m = 4, …, 9, 11$) using the A-D formula [54] in the pressure range 150–180 GPa, which is the experimentally studied pressure region

TABLE II. Parameters of the superconducting state of $P6/mmm$-LaH$_{16}$ at 200–300 GPa calculated using the Eliashberg equation with $\mu^* = 0.41$. Here γ is the Sommerfeld constant calculated using Eq. (2).

Parameter	200 GPa	250 GPa	300 GPa
N$_f$, states/f.u./Ry	7.21	6.94	7.07
λ	1.82	1.63	1.44
$\omega_{\log}$, K	1362	1511	1675
T_C, K	156	141	118
$\Delta(0)$, meV	29.6	25.7	20.2
$\mu_0H_C(0)$, T	35.0	29.9	23.6
$\Delta C/T_C$, mJ/mol K^2	18.6	15.1	12.4
γ, mJ/mol K^2	7.3	6.5	6.1
$R_\Delta = 2\Delta(0)/k_BT_C$	4.5	4.2	4.0

TABLE III. Superconducting parameters of LaH$_{10}$ and LaH$_{16}$ phases

Parameter	LaH$_{10}$ at 200 GPa	LaH$_{16}$ at 200 GPa
Critical temperature (T_C), K	271	156
μ^* (Eliashberg equation)	0.20	0.41
μ^* (Allen–Dynes equation)	0.11	0.198

[27], with the commonly accepted μ^* values (0.1–0.15). We consider this interval of μ^* reasonable because for LaH$_{10}$ and LaH$_{16}$ the A-D formula yielded μ^* equal to 0.11 and 0.2, respectively (Supplemental Material Table S2 [50]). The calculated T_C values are shown in Fig. 4. The results point to LaH$_6$ and LaH$_7$ as the compounds that could correspond to the experimentally observed transition at ~215 K with the critical magnetic field $\mu_0 H_C(0) = 60$–70 T; the other transition at ~112 K with the critical magnetic field $\mu_0 H_C(0) = 20-25$ T could occur in LaH$_5$, LaH$_8$, and LaH$_{11}$. LaH$_4$ with predicted $T_c = 67-87$ K may explain experimental transition at 70 K. More details about the calculation of T_C in these phases can be found in the Supplemental Material [50].

E. Possible departure from the standard Eliashberg picture

In the present analysis, we estimated the superconducting parameters with the A-D formula and isotropic (constant-DOS) Eliashberg equation. They are based on a simple standard view of the detailed electronic structure such as the constant electronic DOS and screened Coulomb matrix elements. The degree of departure of the target system from this simple view can be estimated by analyzing the Coulomb pseudopotential μ^* [51]. We evaluated the nonrenormalized μ as the Fermi surface average of the screened Coulomb interac-

FIG. 4. Superconducting temperatures T_C, obtained using the A-D formula with $\mu^* = 0.1$, and critical magnetic fields for a series of lanthanum hydrides at 150 and 180 GPa.

tion [49,50], which was 0.18 and 0.11 for LaH$_{10}$ and LaH$_{16}$, respectively. The straightforward use of the renormalization formula

$$\mu^* = \mu/[1 + \mu\ln(E_{el}/\omega_D)], \qquad (2)$$

where E_{el} is the Fermi level calculated from the band bottom and ω_D is the Debye frequency, yields $\mu^* = 0.10$ and 0.07, which is far smaller than our estimate from SCDFT (0.20 and 0.41, respectively). The deviation of μ^* estimated using the SCDFT approach from the empirically accepted range 0.10–0.15 [49,57] has been pointed out in the previous SCDFT studies [48,51]. It is thought to indicate the substantial effects ignored in Eq. (2), such as the energy dependence of the electronic DOS and the Kohn-Sham state dependence of the Coulomb matrix element, which are incorporated in the SCDFT framework. Notably, we found a paradoxical relation, $\mu < \mu^*$, derived from the SCDFT, which has also been observed in H$_3$S [58]. The DOS effect would be accounted for more properly by the DOS-dependent Eliashberg equation [59]. However, the single-parameter approximation of the Coulomb effect is likely less reliable in hydrides because of the large phonon energy scale comparable to the electronic one. The *ab initio* treatment of the Coulomb matrix element in the Eliashberg equation [60] would reveal such effects on the superconducting parameters evaluated above, which is out of the scope of the present study.

IV. CONCLUSIONS

Using the *ab initio* evolutionary algorithm USPEX, we have predicted stable superconducting compounds in the La-H system at 50, 100, 150, and 200 GPa, including the previously unknown superhydride $P6/mmm$-LaH$_{16}$. The electronic, phonon, and superconducting properties of LaH$_m$ with $m = 4, \ldots, 11$ were studied within the harmonic approximation, which gives possible explanations of the observed superconducting transitions at 70, 112, and 215 K [27]. The SCDFT calculations for LaH$_{10}$ and LaH$_{16}$ led to unusually high values of μ^* (0.2 for LaH$_{10}$ and 0.41 for LaH$_{16}$) for the numerical solution of the Eliashberg equation, lying far outside the conventionally accepted interval, 0.1–0.15. The Eliashberg function calculated for $Fm\bar{3}m$-LaH$_{10}$ at 170 GPa yields $T_C = 259$ K, according to the numerical solution of the Eliashberg equation with $\mu^* = 0.2$. The critical magnetic field of $Fm\bar{3}m$-LaH$_{10}$ was found to be 89–95 T (73 T for the $R\bar{3}m$ phase), the harmonic isotope coefficient $\beta = 0.48$. The values of all the superconducting parameters for lanthanum hydrides are in close agreement with the available experimental data [27]. We found that $P6/mmm$-LaH$_{16}$ is a high-temperature superconductor with T_C of up to 156 K, the critical magnetic field of ~35 T, and the superconducting gap of 30 meV at 200 GPa. An important conclusion of this investigation is that the μ^* value depends significantly on how exactly it was determined, and especially for the numerical solution of the Eliashberg equation, it may significantly vary and go beyond the commonly accepted interval, 0.1–0.15, which lends a special importance to the SCDFT calculations.
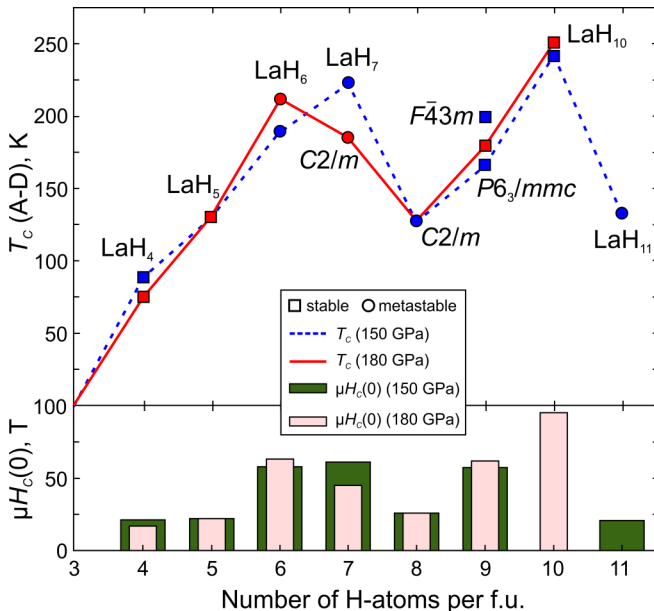
[1] N. W. Ashcroft, Phys. Rev. Lett. **21**, 1748 (1968).

[2] P. Cudazzo, G. Profeta, A. Sanna, A. Floris, A. Continenza, S. Massidda, and E. K. U. Gross, Phys. Rev. Lett. **100**, 257001 (2008).

[3] P. Cudazzo, G. Profeta, A. Sanna, A. Floris, A. Continenza, S. Massidda, and E. K. U. Gross, Phys. Rev. B **81**, 134505 (2010).

[4] P. Cudazzo, G. Profeta, A. Sanna, A. Floris, A. Continenza, S. Massidda, and E. K. U. Gross, Phys. Rev. B **81**, 134506 (2010).

[5] R. P. Dias and I. F. Silvera, Science **355**, 715 (2017).

[6] N. W. Ashcroft, Phys. Rev. Lett. **92**, 187002 (2004).

[7] H. Wang, J. S. Tse, K. Tanaka, T. Iitaka, and Y. Ma, Proc. Natl. Acad. Sci. **109**, 6463 (2012).

[8] H. Liu, I. I. Naumov, R. Hoffmann, N. W. Ashcroft, and R. J. Hemley, Proc. Natl. Acad. Sci. **114**, 6990 (2017).

[9] D. Duan, Y. Liu, F. Tian, D. Li, X. Huang, Z. Zhao, H. Yu, B. Liu, W. Tian, and T. Cui, Sci. Rep. **4**, 6968 (2014).

[10] A. G. Kvashnin, D. V. Semenok, I. A. Kruglov, I. A. Wrona, and A. R. Oganov, ACS Appl. Mater. Interfaces **10**, 43809 (2018).

[11] D. V. Semenok, A. G. Kvashnin, I. A. Kruglov, and A. R. Oganov, J. Phys. Chem. Lett. **9**, 1920 (2018).

[12] W. Zhang, A. R. Oganov, A. F. Goncharov, Q. Zhu, S. E. Boulfelfel, A. O. Lyakhov, M. Somayazulu, and V. B. Prakapenka, Science **342**, 1502 (2013).

[13] A. P. Drozdov, M. I. Eremets, I. A. Troyan, V. Ksenofontov, and S. I. Shylin, Nature (London) **525**, 73 (2015).

[14] I. A. Kruglov, A. G. Kvashnin, A. F. Goncharov, A. R. Oganov, S. S. Lobanov, N. Holtgrewe, Sh. Jiang, V. B. Prakapenka, E. Greenberg, and A. V. Yanilkin, Sci. Adv. **4**, eaat9776 (2018).

[15] D. Duan, Y. Liu, Y. Ma, Z. Shao, B. Liu, and T. Cui, Natl. Sci. Rev. **4**, 121 (2017).

[16] R. J. Hemley, M. Ahart, H. Liu, and M. Somayazulu, arXiv:1906.03462 (2019).

[17] P. P. Kong, A. P. Drozdov, E. Eroke, and M. I. Eremets, in *Book of Abstracts, 18-23rd August 2017, Beijing, China* (AIRAPT 26 joint with ACHPR 8 & CHPC 19, 2017), p. 347.

[18] Z. M. Geballe, H. Liu, A. K. Mishra, M. Ahart, M. Somayazulu, Y. Meng, M. Baldini, and R. J. Hemley, Angew. Chem. Int. Ed. **57**, 688 (2017).

[19] C. M. Pépin, G. Geneste, A. Dewaele, M. Mezouar, and P. Loubeyre, Science **357**, 382 (2017).

[20] A. Majumdar, J. S. Tse, M. Wu, and Y. Yao, Phys. Rev. B **96**, 201107(R) (2017).

[21] A. G. Kvashnin, I. A. Kruglov, D. V. Semenok, and A. R. Oganov, J. Phys. Chem. C **122**, 4731 (2018).

[22] N. P. Salke, M. M. D. Esfahani, Y. Zhang, I. A. Kruglov, J. Zhou, Y. Wang, E. Greenberg, V. B. Prakapenka, J. Liu, A. R. Oganov, and J.-F. Lin, Nat. Commun. **10**, 4453 (2019).

[23] K. Tanaka, J. S. Tse, and H. Liu, Phys. Rev. B **96**, 100502(R) (2017).

[24] G. Gao, R. Hoffmann, N. W. Ashcroft, H. Liu, A. Bergara, and Y. Ma, Phys. Rev. B **88**, 184104 (2013).

[25] K. Abe, Phys. Rev. B **96**, 144108 (2017).

[26] X. Li and F. Peng, Inorg. Chem. **56**, 13759 (2017).

[27] A. P. Drozdov, P. P. Kong, V. S. Minkov, S. P. Besedin, M. A. Kuzovnikov, S. Mozaffari, L. Balicas, F. F. Balakirev, D. E. Graf, V. B. Prakapenka, E. Greenberg, D. A. Knyazev, M. Tkacz, and M. I. Eremets, Nature (London) **569**, 528 (2019).

[28] M. Somayazulu, M. Ahart, A. K. Mishra, Z. M. Geballe, M. Baldini, Y. Meng, V. V. Struzhkin, and R. J. Hemley, Phys. Rev. Lett. **122**, 027001 (2019).

[29] A. R. Oganov and C. W. Glass, J Chem Phys **124**, 244704 (2006).

[30] A. R. Oganov, A. O. Lyakhov, and M. Valle, Acc. Chem. Res. **44**, 227 (2011).

[31] A. O. Lyakhov, A. R. Oganov, H. T. Stokes, and Q. Zhu, Comput. Phys. Commun. **184**, 1172 (2013).

[32] P. V. Bushlanov, V. A. Blatov, and A. R. Oganov, Comput. Phys. Commun. **236**, 1 (2019).

[33] P. Hohenberg and W. Kohn, Phys. Rev. **136**, B864 (1964).

[34] W. Kohn and L. J. Sham, Phys. Rev. **140**, A1133 (1965).

[35] J. P. Perdew, K. Burke, and M. Ernzerhof, Phys. Rev. Lett. **77**, 3865 (1996).

[36] P. E. Blöchl, Phys. Rev. B **50**, 17953 (1994).

[37] G. Kresse and D. Joubert, Phys. Rev. B **59**, 1758 (1999).

[38] G. Kresse and J. Furthmüller, Phys. Rev. B **54**, 11169 (1996).

[39] G. Kresse and J. Hafner, Phys. Rev. B **47**, 558 (1993).

[40] G. Kresse and J. Hafner, Phys. Rev. B **49**, 14251 (1994).

[41] P. Giannozzi, S. Baroni, N. Bonini, M. Calandra, R. Car, C. Cavazzoni, D. Ceresoli, G. L. Chiarotti, M. Cococcioni, I. Dabo, A. D. Corso, S. de Gironcoli, S. Fabris, G. Fratesi, R. Gebauer, U. Gerstmann, C. Gougoussis, A. Kokalj, M. Lazzeri, L. Martin-Samos, N. Marzari, F. Mauri, R. Mazzarello, S. Paolini, A. Pasquarello, L. Paulatto, C. Sbraccia, S. Scandolo, G. Sclauzero, A. P. Seitsonen, A. Smogunov, P. Umari, and R. M. Wentzcovitch, J. Phys.: Condens. Matter **21**, 395502 (2009).

[42] S. Baroni, S. de Gironcoli, A. Dal Corso, and P. Giannozzi, Rev. Mod. Phys. **73**, 515 (2001).

[43] A. Togo and I. Tanaka, Scr. Mater. **108**, 1 (2015).

[44] A. Togo, F. Oba, and I. Tanaka, Phys. Rev. B **78**, 134106 (2008).

[45] M. Lüders, M. A. L. Marques, N. N. Lathiotakis, A. Floris, G. Profeta, L. Fast, A. Continenza, S. Massidda, and E. K. U. Gross, Phys. Rev. B **72**, 024545 (2005).

[46] M. A. L. Marques, M. Lüders, N. N. Lathiotakis, G. Profeta, A. Floris, L. Fast, A. Continenza, E. K. U. Gross, and S. Massidda, Phys. Rev. B **72**, 024546 (2005).

[47] R. Akashi and R. Arita, Phys. Rev. B **88**, 014514 (2013).

[48] J. P. Carbotte, Rev. Mod. Phys. **62**, 1027 (1990).

[49] P. Morel and P. W. Anderson, Phys. Rev. **125**, 1263 (1962).

[50] See Supplemental Material at http://link.aps.org/supplemental/10.1103/PhysRevB.101.024508 for crystal data of La-H phases, electronic, phonon and superconducting properties including Eliashberg spectral functions (n.d.).

[51] G. Profeta, C. Franchini, N. N. Lathiotakis, A. Floris, A. Sanna, M. A. L. Marques, M. Lüders, S. Massidda, E. K. U. Gross, and A. Continenza, Phys. Rev. Lett. **96**, 047003 (2006).

[52] F. Peng, Y. Sun, C. J. Pickard, R. J. Needs, Q. Wu, and Y. Ma, Phys. Rev. Lett. **119**, 107001 (2017).

[53] D. V. Semenok, I. A. Kruglov, A. G. Kvashnin, and A. R. Oganov, arXiv:1806.00865 (2018).

[54] P. B. Allen and R. C. Dynes, Phys. Rev. B **12**, 905 (1975).

[55] D. V Semenok, A. G. Kvashnin, A. G. Ivanova, V. Svitlyk, V. Y. Fominski, A. V. Sadakov, O. A. Sobolevskiy, V. M. Pudalov, I. A. Troyan, and A. R. Oganov, Mater. Today (2019), doi:10.1016/j.mattod.2019.10.005.

[56] K. Momma and F. Izumi, J. Appl. Crystallogr. **44**, 1272 (2011).

[57] K.-H. Lee, K. J. Chang, and M. L. Cohen, Phys. Rev. B **52**, 1425 (1995).

[58] J. Flores-Livas, A. Sanna, and E. K. U. Gross, Eur. Phys. J. B **89**, 63 (2016).

[59] W. E. Pickett, Phys. Rev. B **26**, 1186 (1982).

[60] A. Sanna, J. A. Flores-Livas, A. Davydov, G. Profeta, K. Dewhurst, S. Sharma, and E. K. U. Gross, J. Phys. Soc. Jpn. **87**, 041012 (2018).